NANO LETTERS

2003
Vol. 3, No. 11
1499−1503

Solid Gold Nanostructures Fabricated by Electron Beam Deposition

Kristian Mølhave,*,† Dorte Nørgaard Madsen,† Anne Marie Rasmussen,‡ Anna Carlsson,‡ Charlotte C. Appel,‡ Michael Brorson,‡ Claus J. H. Jacobsen,‡ and Peter Bøggild†

Mikroelektronik Centret, Technical University of Denmark, DK-2800 Kgs. Lyngby, Denmark and Haldor Topsøe A/S, Nymøllevej 55, DK-2800 Lyngby, Denmark

Received July 17, 2003; Revised Manuscript Received September 3, 2003

ABSTRACT

Direct writing with gold by electron beam deposition is a method for rapid fabrication of electrically conducting nanostructures. An environmental scanning electron microscope (ESEM) equipped with a source of the precursor gas dimethylacetylacetonate gold(III) was used to fabricate nanoscale tips and bridges. Transmission electron microscopy was used to study how the composition of these structures was affected when the background gas in the ESEM chamber and the electron beam parameters were varied. The nanostructures were layered composites of up to three different materials each characterized by a certain range of gold/carbon ratios. Above a certain threshold of ESEM chamber water vapor pressure and a certain threshold of electron beam current, the deposited tips contained a solid polycrystalline gold core. The deposition technique was used to fabricate free-standing nanowires and to solder free-standing carbon nanotubes to gold electrodes as well as to other carbon nanotubes.

Introduction. Electron beam deposition (EBD) is an attractive tool for rapid construction of three-dimensional nanostructures with customizable mechanical and electrical properties.[1−3] Typically, in a scanning electron microscope (SEM), a small amount of residual organic gas molecules is present in the chamber. When the electron beam is focused on a surface, the generated secondary electrons decompose the organic gas molecules and a solid carbonaceous tip will grow in the direction of the beam. By slowly scanning the electron beam during deposition, more complex three-dimensional structures can be fabricated.[4] EBD has also been used to attach nanotubes to other structures[5] and to join carbon nanotubes together.[6]

Metal-containing EBD materials can be obtained by introducing an organometallic gas in the chamber. The metal content of the EBD material can be increased by (i) heating the substrate,[7] (ii) using a precursor gas without carbon,[8] or (iii) introducing an additional gas such as water vapor while using an *environmental* scanning electron microscope (ESEM).[9,10] Recently, we demonstrated low contact resistance soldering of carbon nanotubes onto microelectrodes using organometallic EBD in an ESEM.[11] Folch et al. investigated EBD in an ESEM with dimethyl(hexafluoroacetylacetonate) gold(III) as precursor gas.[9] Using Auger electron spectroscopy they found that the gold content of tips could be increased to 50% by using 10 Torr 80%Ar/20%O_2 as chamber gas. However, Auger electron spectroscopy mainly probes the outermost atomic layers (a few nanometers) of the typically 20−200 nm wide structures.

In this article we report controlled EBD in an ESEM of nanostructures with solid gold cores. The influence of various parameters on the structure and composition of the deposited material was investigated by high-resolution TEM (HRTEM). It was found that the presence of water vapor in the ESEM chamber plays a crucial role in obtaining dense, polycrystalline gold cores.

Experimental Methods. The deposition setup was installed in a Philips XL30 ESEM equipped with a field emission electron gun. All experiments were performed at room temperature using the precursor gas dimethylacetylacetonate gold(III), [$Au(CH_3)_2(C_5H_7O_2)$]. The solid source material (vapor pressure 0.01 Torr equal to 1.3 Pa at 25 °C) was placed in a small aluminum cylinder mounted on a nozzle with a 10 mm long, 1 mm diameter bore, ending about 1 mm from the TEM grid that served as the deposition target. The cylinder was loaded with 50 mg freshly crushed [$Au(CH_3)_2(C_5H_7O_2)$] crystals before each ESEM session, but the lifetime of the source varied substantially. Thus, tip growth rates could vary as much as a factor of 2 from session to session. Each graph presented in this paper is based on data from within one single session. Without precursor gas

* Corresponding author. E-mail: krm@mic.dtu.dk.
† Mikroelektronik Centret.
‡ Haldor Topsøe A/S.

10.1021/nl034528o CCC: $25.00
Published on Web 10/01/2003

present in the chamber, the deposition rate was negligible in the high vacuum mode as well as in the gas mode of the ESEM.

The dependence of the EBD tip structure and composition on the various experimental parameters was investigated. Before deposition of a tip, the electron beam was focused to the smallest possible spot at the given experimental parameters. During deposition, the beam was kept in the same position for 120 s. The working distance was maintained at 10 mm in all experiments. The beam current was controlled by changing the strength of the condensor lens (i.e., spot size), and its magnitude was estimated by placing an electrically conducting plate in the beam path and measuring the absorbed current in high vacuum mode. This is not a strictly correct measure of the beam current but for the present purposes the method is adequate. In the experiments, gas type, pressure, working distance, and temperature were kept constant when beam current was changed. Therefore, under the given conditions the ratio I/I_0 (where I_0 is the intensity of the electron beam in a vacuum and I is the intensity of the unscattered part of the beam) is expected to be constant.[12] Analysis of the deposited tips was made by HRTEM at 200 kV in a Philips CM200 FEG UltraTwin.

Results. During a deposition session, the tip height grew with a constant rate of up to 1.5 μm/minute, which is comparable to EBD growth rates reported in the literature.[7,13] The TEM analysis showed that, depending on the ESEM parameters, the deposited tips may contain three distinct types of concentric layers, which we shall refer to as *core*, *crust*, and *contamination layers*. The apices of three tips with different morphologies, all deposited by a beam of 10 kV acceleration voltage and about 0.2 nA beam current, are presented in Figure 1. Tips deposited in 1 Torr N_2 (Figure 1a) consisted of gold nanocrystals (diameter 3−5 nm) embedded in an amorphous carbon matrix; they appear similar to tips fabricated by EBD in a traditional SEM.[14] Tips deposited using 0.9 Torr H_2O vapor as chamber gas (Figure 1b) contained a central core of dense gold surrounded by a crust resembling the material of the tip shown in Figure 1a. The tip presented in Figure 1c was made under similar conditions as the tip in Figure 1b, but in this case a second deposition was made 1.5 μm to the right of the tip shown. This led to the tip becoming covered by a contamination layer, thickest on the side facing the second deposition. The contamination layer consisted of amorphous carbon with lower gold content than the crust. When structures with asymmetric contamination layers were imaged in SEM or TEM, the tips slowly bent toward the side with the thickest contamination layer (Figure 1d).

In HRTEM images of tip cores, crystal grains can often be found over areas much larger than the typical diameter of nanocrystals in the crust, and sometimes even comparable to the core diameter. Figure 2 shows an example of such a tip structure, where lattice patterns are visible across distances much larger than the sizes of the crust nanocrystals. Estimating the upper limit of the size of the core crystal grains is not straightforward because the thicker parts of the cores block the TEM electrons. Fourier transforms of TEM

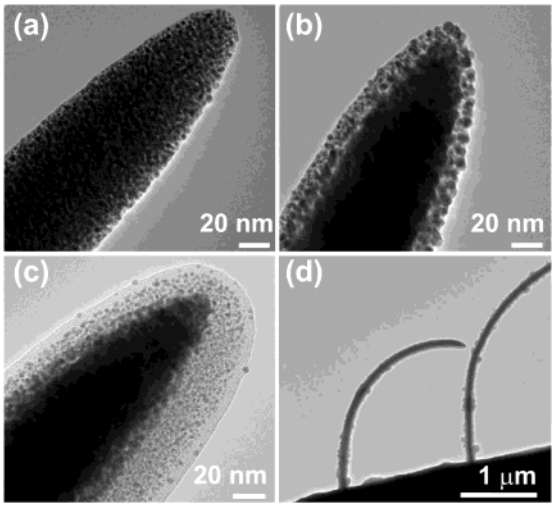

Figure 1. TEM images giving an overview of typical tip structures deposited in an ESEM. (a) Deposition in nitrogen gas; tips consist of gold nanocrystals embedded in an amorphous carbon matrix. (b) Deposition in water vapor; tips consist of a dense core of gold surrounded by a crust of gold nanocrystals in amorphous carbon, i.e., the crust material is similar to the material of the tip in (a). (c) Influence of later deposition nearby; a thick contamination layer covers the tip on the side toward the deposition a few μm to the right. Contamination layers have a lower gold content than the crust material and are thicker on the side facing the later depositions. Further, imaging of structures in ESEM with the source present results in contamination layers of almost pure carbon (the uniform outermost layer of the tip in (c)). (d) Influence on tips with contamination layers of electron radiation in SEM or TEM; irreversible deformation occurs as a bending toward the side with the thickest contamination layer.

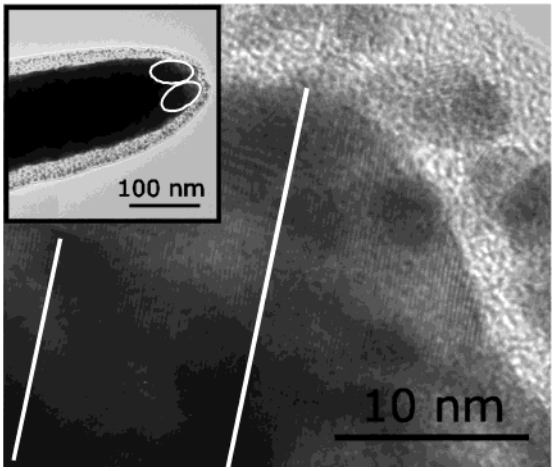

Figure 2. HRTEM image of a tip with a core. The cores often contain large crystal grains visible over distances several times the typical nanocrystal diameter. The two marked areas in the inset show the approximate size and position of two large monocrystalline grains in the tip apex. The higher magnification image show half the upper grain, with the lattice structure indicated by the white lines.

core images show lattice spacings of 2.5, 2.1, and 1.5 Å corresponding to gold lattice spacings 2.35, 2.04, and 1.44 Å, within an uncertainty of approximately 5%, which is expected since the imaging conditions were not optimized for calibrated measurements of lattice spacings. The large crystal domains together with the observed lattice spacings

and EDX spectra indicate that the core consists of solid polycrystalline gold, with grain dimensions significantly larger than the nanocrystals in the crust.

We have examined the dependence of the tip structure on beam acceleration voltage, beam current, and chamber gas pressure. These parameters were varied individually with respect to a default setting of 10 kV acceleration voltage, about 0.2 nA beam current and 0.8 Torr H_2O pressure, which was found optimal in terms of imaging. All tips were deposited in 120 s. The acceleration voltage had little effect on the layer structure except at low energies (<5 kV), where the layer structure became more diffuse. At low acceleration voltages the beam is significantly broadened due to scattering of the primary electrons on the chamber gas. The dependence of the structure on beam current and chamber gas pressure is presented in Figure 3.

The observed structural dimensions for tips deposited at different beam currents are shown in Figures 3a and 3b. Figure 3b shows an increase of the core diameter with beam current. The fit indicates that the core diameter is proportional to the square root of the current.

The type and pressure of the chamber gas used during the deposition also affects tip structure and dimensions (Figure 3c and 3d). The outer (crust) diameter is approximately constant with pressure and similar for H_2O and N_2 (Figure 3c), indicating that the beam is not significantly widened, despite the expected larger scattering of the primary beam at the highest pressures. No cores were observed in the tips deposited in N_2 at any gas pressure. Using water vapor pressures above about 0.4 Torr, the tips contained a solid core surrounded by a crust as shown in Figure 1b, while no cores were seen below this threshold pressure. Both tip height and core diameter appeared to decrease rapidly with decreasing vapor pressure when approaching the threshold. Tips were also deposited using two different gas mixtures, 60%He/40%H_2 and 80%Ar/20%O_2 (both at 2 Torr), where the amounts of O and H in the chamber corresponds to that of water vapor at 0.8 Torr. It was not possible to produce any cores in these experiments, while using water at 0.8 Torr as chamber gas resulted in a core in all experiments.

By scanning the electron beam along a line during deposition, we deposited wires on surfaces as well as from free-standing wires. Using a free-standing carbon nanotube as the starting point, a wire was deposited in the plane perpendicular to the beam by scanning the beam at a speed of a few nm/s (Figure 4a). Like the tips deposited on surfaces, these wires have a core with high gold content. The wire appears to be firmly attached to the carbon nanotube, which was noticeably deformed at the joint. Both the nanotube and the gold wire were covered by a low gold-content contamination layer that arose while imaging at high magnification in the presence of the precursor gas. Figure 4b shows a SEM image of a nanotube soldered to an electrode as reported in ref 11. The line width of such depositions can be down to 20−30 nm, and we have achieved continuous cores with line widths down to 10−20 nm for both fixed and scanned beam depositions (see Figure 3b (and inset), 4a, and 4b).

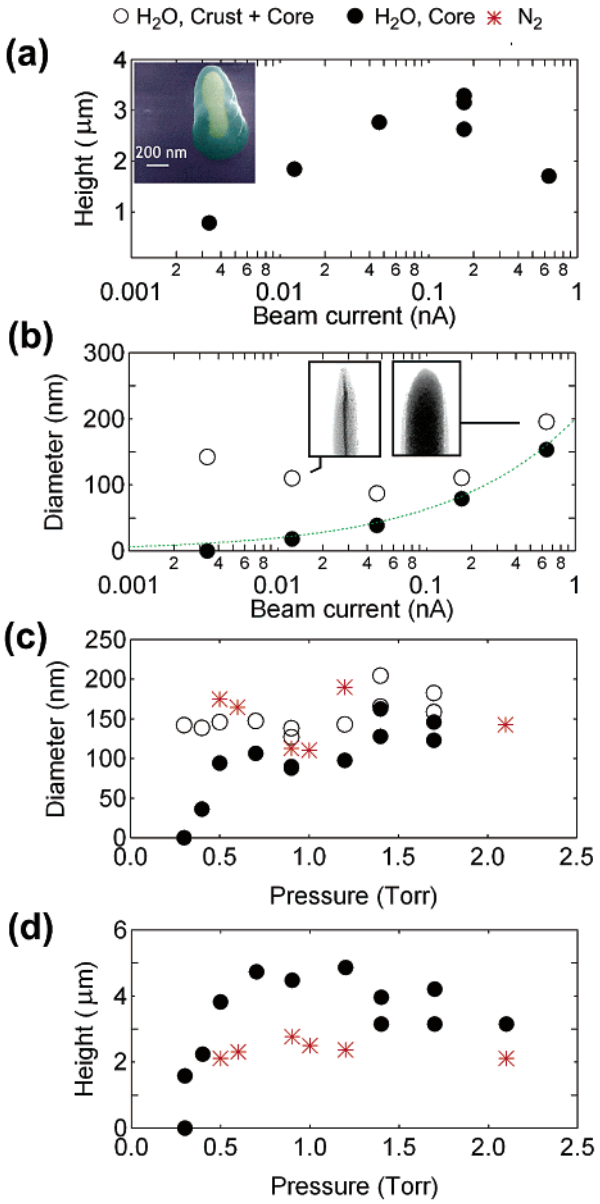

Figure 3. Tip structure as function of beam current, pressure, and type of the chamber gas. All tips were deposited in 120 s using 10 kV acceleration voltage. (a) Tip height (dots) vs beam current with 0.8 Torr H_2O as chamber gas. The inset shows a SEM image of a tip with a crust, which is transparent to the 30 kV SEM beam electrons used for imaging, and a solid core, which appears opaque. (b) Tip diameter (of core (dots) and crust + core (circles)) vs beam current also with 0.8 Torr H_2O as chamber gas. The diameter of the core was proportional to the square root of the current (cf. the curve shown). The insets show TEM images of tips deposited at different currents. (c, d) Tip diameters and heights obtained at different chamber gas types and pressures at a constant primary beam current (0.2 nA).

Discussion. The TEM analyses show that the EBD tips made in ESEM have a unique layer structure, to our knowledge not previously reported in the literature. Three distinct types of layers have been identified: a core, a crust, and carbonaceous contamination layers. From Figures 1a and 1b it is evident that the crust material consists of crystalline particles (3−5 nm diameter) separated by about 1−2 nm. The precursor gas dimethylacetylacetonate gold(III) has a

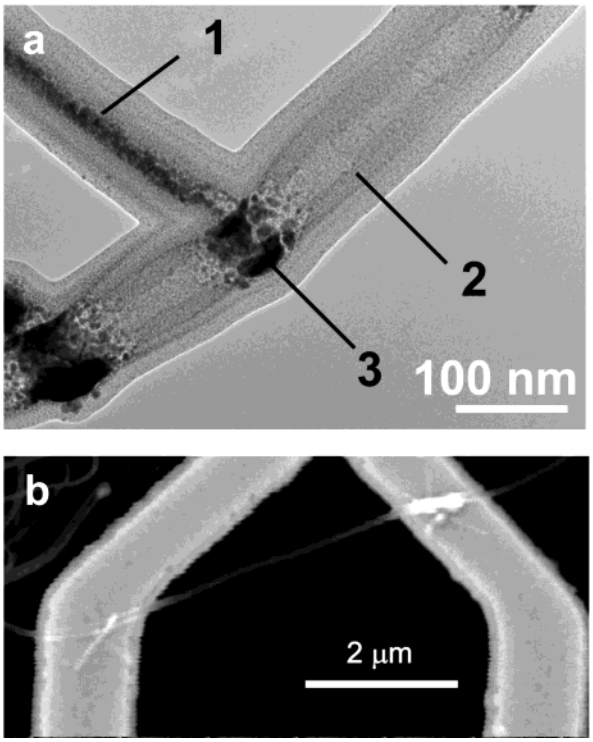

Figure 4. (a) High-resolution transmission electron microscopy image of a joint between a carbon nanotube and a deposited gold wire. The gold wire (1) was made by scanning the beam across a free-standing carbon nanotube (2). Deformation of the nanotube is seen in the joint (3). Both nanotube and gold wire are covered by a 20−30 nm thick contamination layer. (b) An ESEM image of a suspended carbon nanotube soldered onto two gold electrodes by cross-shaped gold depositions. The line width of the depositions is about 20−30 nm. The measured resistance across such bridges is typically in the 10 kΩ range.[11]

C/Au ratio of 7:1. In a solid material consisting of gold spheres with a diameter of 3 nm and graphitic carbon, the gold spheres must be spaced by 1 nm to give the C/Au ratio of the precursor gas. This spacing is consistent with our observations for tips deposited in N_2, in 60%He/40%H_2, and in 80%Ar/20%O_2.

Based on the observed lattice patterns of the cores, with crystal domains much larger than the nanometer-sized crystals commonly seen in the crusts, we find that the cores most likely consist of solid, polycrystalline gold. This is supported by the low resistivity of 10^{-4} Ωcm measured on bridges made of this material, as reported in ref 15. Further, bridges deposited using the chamber gas N_2, which gives no core structure, showed resistivities beyond the measurement sensitivity, i.e., several orders of magnitude higher than the value of ref 15. An extensive study of the mechanical and electrical properties of these structures is in progress. Solid gold cores have been observed with diameters from around 10 nm to 150 nm (Figures 3 and 4). Cores thinner than about 10 nm appear as dense regions with crystallites rather than as continuous solid cores resembling the structure of the core in Figure 4a.

The core diameter can apparently be controlled through the beam current and the water vapor pressure. Compared to deposition in N_2, deposition in the presence of water vapor leads to taller and wider tips as well as a higher gold content, since the gold core takes up a significant fraction of the tip volume. Folch et al. found by Auger electron spectroscopy that oxygen mixtures gave rise to higher gold contents than water vapor.[9] The discrepancy may be explained by the fact that Auger electron spectroscopy probes only the outermost layers of the tips. A minimum requirement for the generation of a core appears to be a water vapor pressure of about 0.4 Torr. We found that the cross-section area of the core was proportional to the beam current (Figure 3b). No gold cores were formed when N_2, O_2/Ar or H_2/He was used as chamber gas, even though the content of O and H in the gas mixtures were comparable to water vapor pressures that consistently gave dense cores. We notice that water is known to influence the diffusion of gold during deposition[16] and that irradiation is capable of affecting the diffusivity of gold clusters.[17]

The tip height appears to decrease at beam currents higher than 0.2 nA and lower than 0.04 nA (Figure 3a). The reason could be that it is difficult to focus at small and large spot sizes (low and high beam currents, respectively). From Figure 3b it seems that at beam currents higher than about 0.05 nA the increase in combined crust and core diameter follows the increase in core diameter. At beam currents lower than 0.05 nA the combined crust and core diameter increases while the core diameter decreases. An explanation may be that as the core diameter decreases, a larger amount of electrons may be able to escape the tip edges and thus cause crust deposition when decomposing precursor gas molecules.

When imaging at very high resolution and in the presence of the gold precursor gas, an outer layer of almost pure carbon, a so-called contamination layer, formed on the deposited structures. Also, when depositing groups of closely spaced tips, a similar layer with very low gold content was observed on the deposited tips at the side that had later faced the beam. The deposition rate in the absence of the precursor gas source was negligible, indicating that the formation of these contamination layers is due to the precursor gas. The contamination layers appeared to induce stress in the tip structures when exposed to electron radiation during imaging in SEM or TEM. The structures were seen to bend toward the side with the thickest contamination layer and retained the bent shape after being exposed to air. This phenomenon has not been reported in earlier work, although we have observed a similar behavior for carbonaceous tips made by EBD from the background gas in a traditional SEM. Mechanically tuning the shape of nanostructures by exposing irradiation-sensitive layers is an intriguing possibility. Preliminary experiments using a controllable source that can be closed when deposition is undesired, show that the thickness of contamination layers can be reduced drastically, thereby also reducing the deformation effect during subsequent imaging.

The EBD method provides the unique possibility of directly forming electrical and mechanical interconnections between free-standing carbon nanotubes and other micro- and nanostructures. The TEM images of nanotube soldering show that the gold connections deform or collapse the nanotube in the joint, which may damage the graphitic layer-

structure of the nanotube close to the solder material. How this affects the electrical properties of the nanotube remains to be investigated.[15] Also, depositions of material on surfaces may give rise to a different material structure, since the surface influences the generation of secondary electrons, which play an important role in the deposition process.[18]

The fast construction of three-dimensional solid gold nanostructures could find applications in many areas of nanotechnology. Apart from rapid prototyping and wiring of electrically conducting structures with potential use as wires, field emitters, strain gauges or thermal sensors (depending of composition), the method has already proven useful for soldering of nanotubes.[11] Furthermore, gold can easily be functionalized to modify the chemical properties of the surface, which may be used to make scanning probe microscopy tips with tailored friction, adhesion or conducting properties.

Acknowledgment. Technical assistance from Sven Ullmann and carbon nanotube samples fabricated by Ramona Mateiu are greatly appreciated. We thank Rodney Ruoff for valuable discussions. The research was supported by the Danish Technical Research Council through a "Talent-projekt" grant.

References

(1) Edinger, K.; Gotszalk, T.; Rangelow, I. W. *J. Vac. Sci. Technol. B* **2001**, *19*, 2856.
(2) Koops, H. W. P.; Weber; M., Schossler, C.; Kaya, A. *SPIE* 1996, *2780*, 388.
(3) Boggild, P.; Hansen, T. M.; Tanasa, C.; Grey, F. *Nanotechnology* **2001**, *12*, 331.
(4) Ooi, T.; Matsumoto, K.; Nakao, M.; Otsubo, M.; Shirakata, S.; Tanaka, S.; Hatamura, Y. *Proceedings of the IEEE Micro Electro Mechanical Systems (MEMS)* **2000**, 580.
(5) Yu, M.-F.; Lourie, O.; Dyer, M. J.; Moloni, K.; Kelly, T. F.; Ruoff, R. S. *Science* **2000**, *287*, 637.
(6) Banhart, F. *Nano Lett.* **2001**, *1*, 329.
(7) Koops, H. W. P.; Schossler, C.; Kaya, A.; Weber, M. *J. Vac. Sci. Technol. B* **1996**, *14*, 4105.
(8) Utke, I.; Hoffman, P.; Dwir, B.; Leifer, K.; Kapon, E.; Doppelt, P. *J. Vac. Sci. Technol. B* **2000**, *18*, 3168.
(9) Folch, A.; Tejada, J.; Peter, C. H.; Wrighton, M. S. *Appl. Phys. Lett.* **1995**, *66*, 2080.
(10) Folch, A.; Servat, J.; Esteve, J.; Tejada, J. *J. Vac. Sci. Technol. B* **1996**, *14*, 2609.
(11) Madsen, D. N.; Molhave, K.; Mateiu, R.; Rasmussen, A. M.; Brorson, M.; Jacobsen, C. J. H.; Boggild, P. *Nano Lett.* **2003**, *3*, 47.
(12) Danilatos, G. D. *Mikrochim. Acta* **1994**, *114/115*, 143−155.
(13) Koops, H. W. P.; Kaya, A.; Weber, M. *J. Vac. Sci. Technol. B* **1995**, *13*, 2400.
(14) Kretz, J.; Rudolph, M.; Weber, M.; Koops, H. W. P. *Microelectron. Eng.* **1994**, *23*, 477.
(15) Madsen, D. N.; Molhave, K.; Mateiu, R.; Boggild, P.; Rasmussen, A. M.; Appel, C. C.; Brorson, M.; Jacobsen, C. J. H., to appear in *Proceedings of the 2003 Third Conference on Nanotechnology* **2003**.
(16) Harsdorff, M. *Thin Solid Films* **1984**, *116*, 55.
(17) Xue, B.; Chen, P.; Hong, Q.; Lin, J.; Tan, K. L. *Mater. Chem.* **2001**, *11*, 2378.
(18) Silvis-Cividjian, N.; Hagen, C. W.; Leunissen, L. H. A.; Kruit, P. *Microelectronic Engineering* **2002**, *61−62*, 693−699.

NL034528O